Bulletin of Geophysics and Oceanography Vol. XX, n. X, pp. XXX-XXX; Xxxxx 20xx
DOI 10.4430/bgo00459

Monitoring and modelling moraine landslides: an example from Cazzaso village (Carnic Alps, Italy)

L. Tunini[1], D. Zuliani[1], F. Di Traglia[2,3], L. Borselli[4,5], C. de Luca[3], T. Nolesini[6] and F. Casu[3]

[1] *Istituto Nazionale di Oceanografia e di Geofisica Sperimentale - OGS, Sgonico (Trieste), Italy*
[2] *Istituto Nazionale di Geofisica e Vulcanologia, Osservatorio Vesuviano, Napoli, Italy*
[3] *Istituto per il Rilevamento Elettromagnetico dell'Ambiente, Consiglio Nazionale delle Ricerche, Napoli, Italy*
[4] *Instituto de Geologia, Universidad Autonoma de San Luis Potosì, San Luis Potosí, Mexico*
[5] *Istituto di Ricerca per la Protezione Idrogeologica, Consiglio Nazionale delle Ricerche, Perugia, Italy*
[6] *Centro per la Protezione Civile, Università degli Studi di Firenze, Firenze, Italy*

(Received: 11 August 2023; accepted: 15 April 2024; published online: 12 July 2024)

ABSTRACT Landslides in Alpine valleys pose significant hazards due to potential impacts on inhabited areas and landslide-dam formation. These valleys feature diverse glacial deposits (moraine, debris talus, and glacio-fluvio-lacustrine materials) with varying technical traits. A comprehensive study investigated a Carnic Alps landslide in north-eastern Italy, focusing on moraine deposits. This entailed geological-geomorphological analyses, slope deformation monitoring, and utilisation of 2D and 3D stability models. The 19th-century landslide occurred in Tolmezzo, Friuli Venezia Giulia, and affected the Cazzaso village. Geological-geomorphological studies involved LiDAR-derived terrain models, borehole-based slope stratigraphy, and inclinometer-derived landslide characterisation. Deformation data combined GPS measurements and multi-temporal interferometric synthetic aperture radar. Reconstructing the slope's geological model, stability assessments employed 2D and 3D limit equilibrium methods, factoring in groundwater and seismicity. Validation occurred against monitoring data and geological-geomorphological observations. The 3D models further identified most landslide-susceptible zones.

Key words: landslides, cost-effective GNSS, multi-temporal InSAR, slope stability analysis.

1. Introduction

Landslides that involve moraine deposits, formed by the advancement and retreat of glaciers, present potential hazards in Alpine regions, directly impacting inhabited villages and towns. Lateral moraine landslides can lead to the formation of landslide-dams, triggering chain effects such as the creation of dam lakes, breaching of dams, and downstream flooding (Korup and Tweed, 2007; Shulmeister *et al*., 2009; Fan *et al*., 2020; Pánek *et al*., 2020; Gao *et al*., 2023). Glacial deposits, particularly moraines, consist of heterogeneous materials with significant variations in technical properties, ranging from glaciolacustrine silt and clay deposits to sands and gravels containing large blocks resulting from lateral rockfalls and glacial transport (Novotný and Klimeš, 2014; Klimeš *et al*., 2016; Perkins *et al*., 2017). While studies on the stability of

glacial deposits, specifically moraines, are relatively scarce, this topic has gained increasing attention, especially considering the rapid retreat of mountain glaciers and the accumulation of recently formed deposits. Over the years, research on the stability of glacial deposits has emphasised the pronounced heterogeneity of material characteristics, primarily attributed to granulometric variations spanning from clay to boulders, reflecting transport and deposition mechanisms (Springman *et al*., 2003; Novotný and Klimeš, 2014; Klimeš *et al*., 2016; Perkins *et al*., 2017). Some studies have highlighted the significance of fine materials within moraine deposits (Novotný and Klimeš, 2014; Klimeš *et al*., 2016), while others have demonstrated the influence of internal stratification and the presence of low-strength layers as primary controls on landslide volume (Baum *et al*., 2005; Perkins *et al*., 2017).

In an effort to propose mitigation strategies for hazards associated with the instability of lateral moraine deposits in Alpine regions, this study presents the results of mapping, monitoring, and modelling efforts focused on a landslide in the south-eastern sector of the Alps, specifically the Carnic Alps in north-eastern Italy (Fig. 1). The study area encompasses moraine deposits as well as slope deposits, including a paleo-landslide. The affected landslide area includes the village of Cazzaso, which falls within the municipality of Tolmezzo, with residential areas situated immediately below the terrace (Fig. 2). The But River, a stream characterised by damming phenomena and fluvial captures during the post-glacial period, is also present in the vicinity (Venturini and Discenza, 2020).

The analyses conducted in this study encompass several components: i) geological-technical reconstruction of slope stratigraphy based on borehole data, including inclinometers for identifying slip surfaces; ii) reconstruction of the hydrogeological structure through analysis of piezometer data obtained from the boreholes; iii) ground displacement monitoring utilising a network made of single-frequency Global Positioning System (GPS) and of high-cost Global Navigation Satellite Systems (GNSS) sensors and Interferometric Synthetic Aperture Radar (InSAR) data; iv) slope stability modelling using the Limit Equilibrium Method (LEM) in both 2D and 3D analyses.

The methodology presented in this research involves the comparison of stability analytical models utilising the LEM in both 2D and 3D dimensions. This is complemented by the incorporation of displacement data sourced from inclinometers, single frequency GPS sensor networks, dual frequency GNSS sensor networks, and Interferometric InSAR data. This comprehensive approach facilitates the reciprocal validation of model outcomes and the interpretation of displacement data. More specifically, the initial analysis of stability in 2D was substantiated by the outcomes derived from 3D models. The validity of the analytical models was further affirmed through the integration of displacement data, enabling the reconstruction of the deformation field of the slope. The 2D stability analysis, performed on hypothetical sliding surfaces, not only corroborated the findings of the 3D models but also contributed to the meaningful interpretation of displacement data.

2. Case study

The study area, situated in the Carnic Alps between NE Italy and southern Austria (Fig. 1), is part of the eastern sector of the Alpine mountain chain. It is characterised by the presence of the external non-to low-metamorphic portion of the Variscan substratum of the Southern Alps, which reflects the complex Variscan and Alpine deformational history (Brime *et al*., 2008; Pasquarè Mariotto and Venturini, 2019). The collision between the Adria microplate and

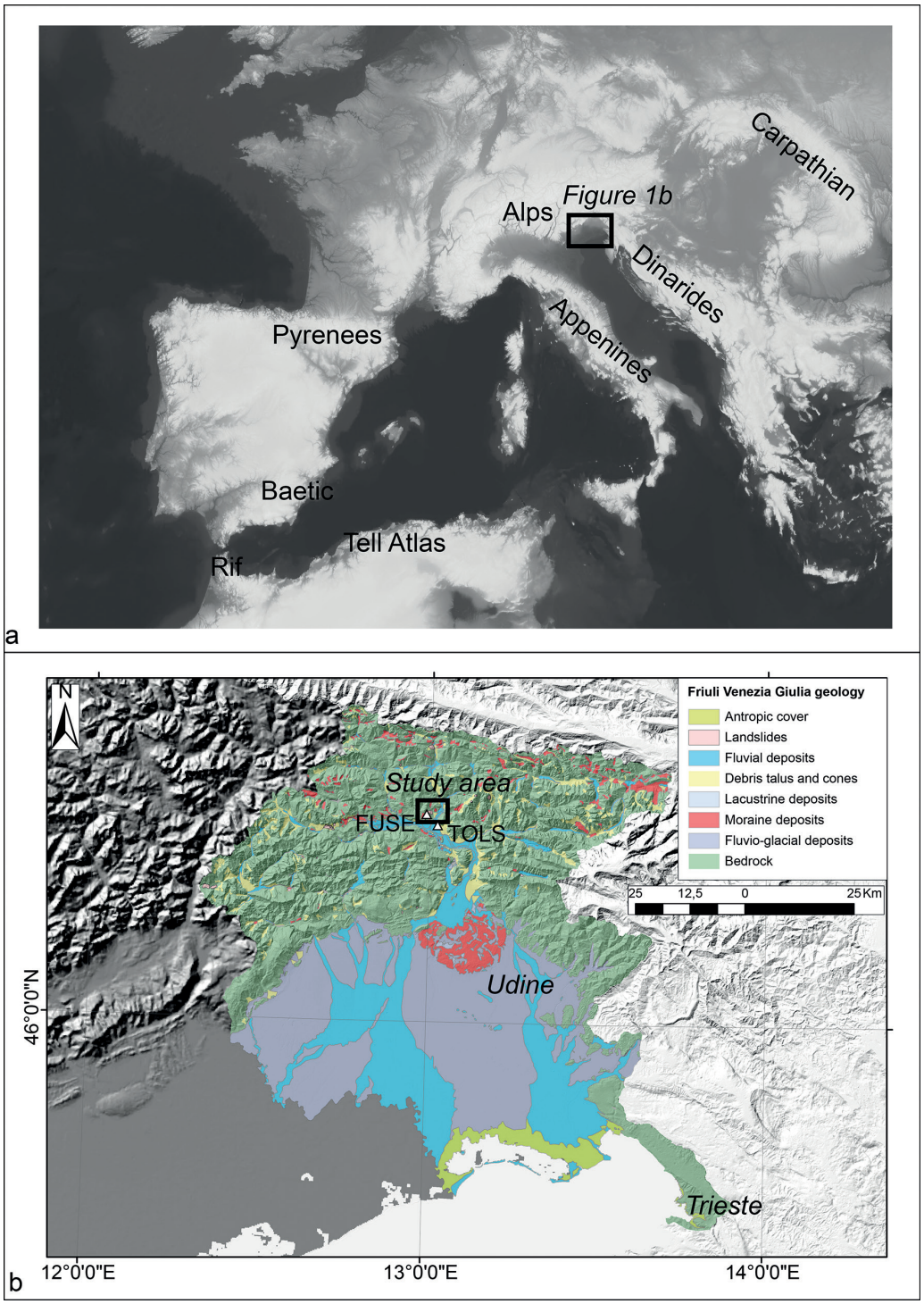

Fig. 1 - a) Geographic location of the study area, in the south-eastern Alps. b) Geological maps of the Friuli Venezia Giulia region, highlighting the presence of moraine deposits in the study area (modified from https://www.regione.fvg.it/rafvg/cms/RAFVG/ambiente-territorio/geologia/FOGLIA01/ and Pondrelli *et al*., 2020). FUSE and TOLS are reference GNSS networks belonging to the FReDNet permanent network of the Institute of Oceanography and Applied Geophysics - OGS [more info can be found in Zuliani *et al*. (2018) and Tunini *et al*. (2024)]. In panel b, the key: anthropic cover.

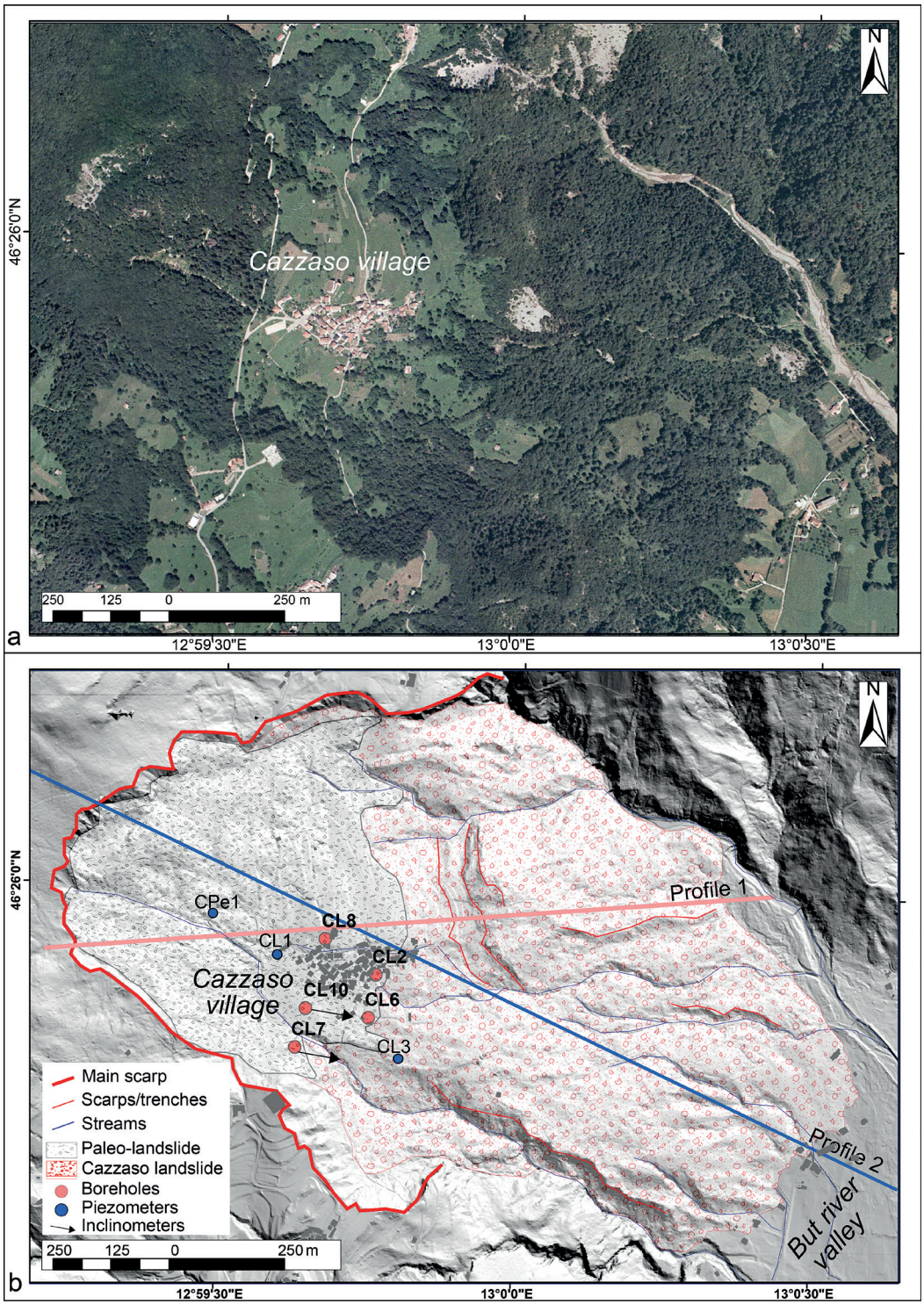

Fig. 2 - Orthophotograph (a) and map (b) of the Cazzaso landslide (modified after Ubertini, 1990). The location of the boreholes has also been reported, distinguishing those equipped with piezometers and those with inclinometers. The location of the two profiles of Fig. 6 has also been reported. Background image: shaded relief model based on a Digital Elevation Model (DEM) derived from LiDAR (Light Detection and Ranging) data of the Cazzaso village area (source: https://irdat.regione.fvg.it/consultatore-dati-ambientali-territoriali/home?language=it).

Eurasia, resulting from the counter-clockwise rotation of Adria, has created the active collision zone with NW-SE oriented Dinaric overthrusts and E-W oriented Alpine thrusts (Anderson and Jackson, 1987; Castellarin and Cantelli, 2000; Magrin and Rossi, 2020). The tectonic history in the area can be divided into three phases: i) the Dinaric NE-SW compressional stage (Mesoalpine) since the Upper Cretaceous-Paleogene, which formed south-westward folds and thrusts; ii) the Insubric NNE-SSW compressional phase (Neo-Alpine) during the Chattian-Burdigalian period, which displaced the Dinaric thrusts and partially reactivated and counter-clockwise rotated their fronts; iii) the Valsuganese NNW-SSE compressions phase (Serravalian-Tortonian age), which generated WSW-ENE-oriented thrusts and back thrusts (Ponton, 2010).

The study area has experienced several strong earthquakes (M > 5) over the centuries, including some notable events in the last century [Tolmezzo in 1928, Cansiglio in 1936, Gemona in 1976 (Slejko *et al*., 2011)]. During the mainshock of 1976, a peak ground acceleration (*PGA*) of >0.19 g was recorded by a sensor near the area of interest (Barnaba *et al*., 2007). The seismic sequence triggered several landslides, but no movements were reported for the Cazzaso landslide (Govi, 1977; Alvioli *et al*., 2024).

The Quaternary deposits in the area consist of glacial, fluvio-glacial, lacustrine, and fluvial sediments, representing different glacial-interglacial phases (Desio, 1926; Colucci *et al*., 2014, 2016). The Last Glacial Maximum resulted in extensive glaciation, and small glaciers and rock glaciers can still be found at elevations between 1830 and 2340 m a.s.l. (Serandrei Barbero *et al*., 1989; Ehlers and Gibbard, 2004; Monegato *et al*., 2007; Carton *et al*., 2009; Carturan *et al*., 2013; Colucci *et al*., 2014, 2016).

The presence of the Cazzaso landslide (Fig. 2) was already observed in the second half of the 19th century, with earlier reports dating back to 1807 and reactivation occurring in October 1851. The landslide caused the displacement of the entire village by 24 m and the destruction of some buildings (CNR-GNDCI, 1992). As a result, the village was partially relocated to a new location 1 km away (Cazzaso Nuova). The study area is situated in the But River valley, a tributary of the Tagliamento River, which is one of the major rivers in the south-eastern Alps and flows through the Friuli Venezia Giulia region (Scaini *et al*., 2021).

3. Materials and methods

In this work, the stratigraphy and technical features of the slope material have been reconstructed by means of 10 borehole data (Fig. 2). Furthermore, to individuate and reconstruct the sliding surface, seven inclinometers were installed. Additionally, the ground displacement, deriving from a cost-effective GPS data and multi-temporal InSAR data, have also been analysed. The latter derive from the Sentinel-1 (S-1) constellation of the European Copernicus program and have been processed using the Parallel Small Baseline Subset (P-SBAS) algorithm (Casu *et al*., 2014; Manunta *et al*., 2019). These data allowed reconstructing a geological-technical model of the slope, which has been used to perform two types of landslide analytical modelling: 2D and 3D LEM modelling. The 2D LEM modelling has been used to quantitatively define the instability of the Cazzaso landslide, considering the variability of the geotechnical parameters, the hydrogeological structure, and the possible seismic load due to the strong regional seismicity. The results have been used to calibrate a 3D LEM model, which, then, allowed us to define areas with different slope stability.

3.1. Borehole data

Boreholes have been drilled over the years since 1979, in order to obtain data on the stratigraphic, geotechnical, and hydrogeological setting of the slope. The boreholes are equipped with (fixed or mobile probe) inclinometers (see Table 1 for details) and/or piezometers. The detection of the depth at which evidence of movement has been found was based mainly on inclinometer data (only at CL7 and CL10, see Fig. 2b). The deeper borehole (CL10), performed with continuous coring, was used to characterise the material by scissometric (Torvane) and penetrometric (Pocket Penetrometer) tests, thanks to which it was possible to define the internal friction angle (φ') and the cohesion (c') of the sampled material, following Mayne (2001), Jaeger *et al*. (2007), Alejano *et al*. (2010), and Alejano and Carranza-Torres (2011). The list of boreholes is shown in Table 1, while their locations are reported in Fig. 2.

Table 1 - Boreholes drilled in the survey area and summary of the installed instrumentation. "Site" pertains to the drilling location as depicted in Fig. 3. "Type of measurement" specifies the instrumentation employed or the nature of the observations conducted at the well. "Date of installation/drilling" denotes the date on which the well was drilled or equipped. "Available/not available" indicates the availability of data for the particular measurement.

Site	Type of measurement	Date of installation/drilling	Available/not available
CL1	Inclinometric	August 1991	Not available
	Piezometric		Available
CL2	Inclinometric	May 1979	Available
CL3	Inclinometric	June 1991	Not available
	Piezometric		Available
CL6	Weather station	July 1991	Available
	Inclinometric		Available
	Piezometric		Available
CL7	Inclinometric	August 1991	Available
	Piezometric		Available
CL8	Inclinometric	September 1994	Available
	Piezometric		Available
CPE1	Piezometric	July 1997	Available
L10	Inclinometric	August 2003	Available
	Geotechnical characterisation		Available

3.2. Cost-effective GPS network

The cost-effective GPS monitoring system (Fig. 3) is composed of 12 single-frequency GPS stations [from GPS1 to GP12 (Zuliani *et al*., 2022a)], and 1 permanent dual-frequency GNSS (Trimble NetR9 model) station located in the village of Cazzaso (CASO). The dual-frequency station tracks both L1 and L2 carrier signals, while the single-frequency devices are able to track only the L1 carrier from the GPS satellites. Nevertheless, if their data are combined with respect to a closer GNSS reference station [FUSE, located at less than 5 km far, or TOLS, used in case of unexpected failure of FUSE station, see Fig. 1b; further information can be found on www.crs.ogs.it/frednet, Battaglia *et al*. (2003), Rossi *et al*. (2016, 2018), Zuliani *et al*. (2018), and Bragato *et al*. (2021)], their capacity of positioning, in post-processing mode, reaches centimetre and millimetre-level repeatability for hourly and daily sessions, respectively (Zuliani *et al*., 2022a).

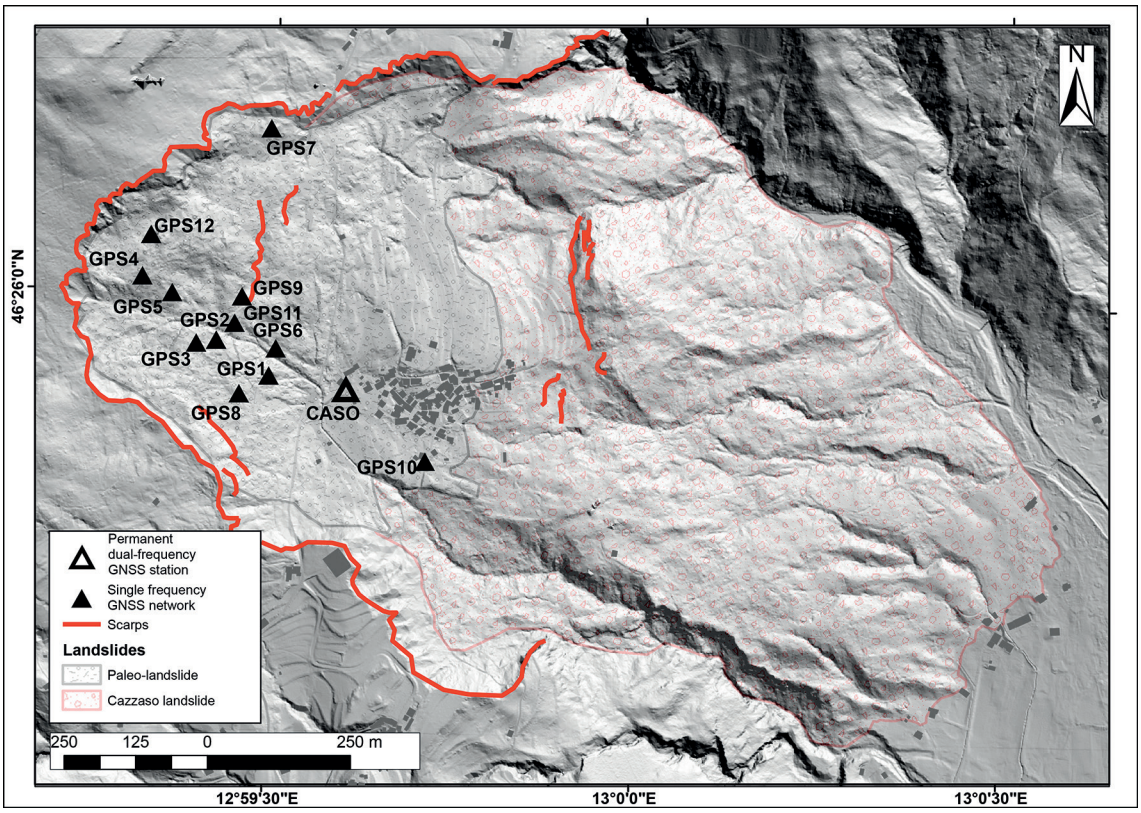

Fig. 3 - Cost-effective GPS monitoring network active on the Cazzaso landslide.

The GPS station network consists of two different types of stations: the node station (NS), which receives the GPS signal and can transmit it only to the gateway, and the gateway station (GW), which is capable not only of retrieving its own GPS signal, but also of collecting the information deriving from the other node stations located nearby and sending them all to a central server (Zuliani *et al*., 2022a, 2022b). The information, between NSs and GWs, travels through a UHF radio at 868 MHz. The data coming from the GW are addressed through a Long-Term Evolution fourth-generation wireless (LTE 4G) modem to a remote server. Details on installation procedures and instrumentation can be found in Zuliani *et al*. (2022a, 2022b). The system adopted for the configuration and control of the GPS network, as well for the data elaboration, called DISPLAYCE, is a cost-effective solution dedicated to monitoring and early-warning of critical infrastructures and areas subject to slope instability (www.yetitmoves.it/). DISPLAYCE software calculates the displacement of each station at regular intervals (i.e. regular sessions) of 1, 3, 6, 12, and/or 24 hours, providing different parameters of the GPS signal (signal-to-noise ratio, number of cycle slips, etc.). The calculation of the displacements is the result of the GPS data processing, which is carried out through the widely-known double difference (DD) technique (Kaplan and Hegarty, 1996; Hofmann-Wellenhof *et al*., 2001). The DD technique is based on the contemporary presence of at least two stations: a rover unit located on the monitored structure, and a master station located outside of it, on a stable structure. The DD technique allows to infer the distance between the rover and master, called baseline. In our study, the rover is represented by each one of the GPS stations located on the Cazzaso landslide (NS or GW stations), whereas the master is the FUSE station located approximately 2.3 km away

from the landslide (Zuliani *et al*., 2022a), belonging to the permanent geodetic network FReDNet (Zuliani *et al*., 2018, 2022a; Tunini *et al*., 2024).

3.3. Multi-temporal InSAR

In this work, a parallel version of the Small Baseline Subset [SBAS (Berardino *et al*., 2002)], referred to as P-SBAS (Casu *et al*., 2014; Zinno *et al*., 2015, 2017; Manunta *et al*., 2019), has been used to generate deformation time-series and corresponding velocity maps for each coherent pixel of the investigated scene, with accuracies of about 5-10 mm and 1-2 mm/yr, respectively.

To analyse the ground deformation of the study area, we processed through the P-SBAS algorithm 256 and 267 S-1 data acquired from ascending (Track 44) and descending (Track 95) orbits, respectively, in the June 2016 - February 2021 interval. The single LOS (Line of Sight) measurements were then combined according to Casu and Manconi (2016), to retrieve the vertical and E-W ground displacement components.

3.4. Landslide analytical modelling

To analyse the stability of 2D slopes, the Slope Stability Analysis Program [SSAP (Borselli *et al*., 2011; Borselli, 2022)] was utilised. The factor of safety (*FS*) was determined using the Morgenstern-Price method (Morgenstern and Price, 1965), while the identification of critical surfaces was conducted through the implementation of the Random Search engine, which generated potential sliding surfaces using Monte Carlo methods (Borselli, 2022; Di Traglia *et al*., 2023a, 2023b; Innocenti *et al*., 2023). Within SSAP, a feature known as the "Dynamic Surface Search Attractor" was incorporated to gradually narrow down the initial research zone based on the progressively recognised surfaces with lower *FS*.

SSAP generates graphical representations of surfaces with the lowest *FS*, as well as internal distributions of forces and pressure, the distribution of local *FS*, and the local distribution of the numerical reliability of the general *FS* solution (referred to as the RHO index). Additionally, SSAP produces:

- a 2D colour map depicting the distribution of average local *FS* obtained through local stress distribution. This is achieved by employing a quasi-Finite Element Analysis Model [qFEM: (Borselli, 2022; Di Traglia *et al*., 2023a, 2023b)] that implements classical finite element procedures (Schofield and Wroth, 1968; Griffiths and Lane, 1999). The colour map describes the local distribution of *FS* and includes a representation of the likely direction of plasticisation in areas where *FS* is less than 1;
- an over stress ratio (OSR) map based on the approach proposed by Farias and Naylor (1998). This map highlights areas where the maximum local shear stress exceeds the local shear strength (Borselli, 2022; Di Traglia *et al*., 2023a, 2023b). Areas with OSR values greater than 1.0 are considered more prone to experiencing progressive failure.

The slope stability analysis was conducted along two profiles with different orientations to accurately assess the slope stability (see profiles in Fig. 2b). Profile selection took into consideration two factors: i) the presence of deformation structures such as scarps and trenches (Profile 1), and ii) the maximum extent of the landslide (Profile 2). Topographic profiles were derived from the LiDAR DEM (1×1 m^2 pixel resolution; source: irdat.regione.fvg.it/consultatore-dati-ambientali-territoriali/home?language=it) and resampled at 25-metre intervals to create a smoother surface, disregarding smaller and localised instability phenomena. For Profile 1, tests were performed with varying aquifer depths to account for changes in the piezometric

surface due to meteorological events (max variation = 10 m). Profile 2 considered a single 'high' piezometric surface, addressing critical scenarios.

In terms of loading conditions, the 2D slope stability analysis was conducted under static and dynamic conditions. For the dynamic stability analysis, SSAP employed the pseudo-static method and seismic coefficients. The horizontal force applied to the centroid of each wedge was determined as $F = Kh \cdot W$, where Kh represents the horizontal seismic coefficient and W denotes the weight of the wedge. Kh is a function of the maximum horizontal acceleration and the topographical and lithological properties of the site. The vertical seismic coefficient Kv was assumed as $Kv/kH = 0.5$. The maximum horizontal seismic coefficient, Kh, was 0.07 g, comparable to the maximum ground acceleration recorded in the area during the 1976-1977 seismic sequence (Barnaba *et al*., 2007). So, the final seismic coefficients used in SSAP were $Kh = 0.07$ g and $Kv = 0.035$ g.

The 3D slope stability modelling was performed using the Scoops3D software (Reid *et al*., 2015). This software evaluates slope stability based on a digital topography (in this case, the resampled LiDAR DEM) using a 3D column approach that assesses the stability of numerous potential failure surfaces within a user-defined volume range (Reid *et al*., 2000, 2015; Baum *et al*., 2005). Stability analysis for rotational and spherical landslide surfaces was conducted using a 3D version of Bishop's simplified method (Reid *et al*., 2000, 2015). In addition to calculating the 3D *FS* value and to identify the most critical surface (lowest *FS*), Scoops3D also provides information on the volume and area associated with each potential landslide (Reid *et al*., 2000, 2015).

The numerical code offers the option to represent subsurface materials with full 3D distributions of: i) internal friction angle (φ'), cohesion (c'), and weights (γ_{unsat} and γ_{sat}); ii) earthquake or seismic loading effects in pseudo-static analyses; iii) pore-water pressure effects using pore-pressure ratios (relative to vertical stresses), a piezometric surface, or a full 3D distribution of pressure heads; or iv) fully 3D variably saturated groundwater flow fields and the effects of unsaturated suction stresses.

The reconstruction of the 3D geometry of the lithology has been performed using the data of the boreholes, together with the geological reconstruction of the surface, and the morphological elements of the slope. The basal boundary between the bedrock and moraine/slope deposits was obtained by interpolating the slope upstream and downstream of the landslide, using a series of topographic-lithological profiles, including the two profiles used for the 2D stability calculation using SSAP, and interpolating the landslides edge using the methodology proposed by Paulin *et al*. (2022). Although this simplification introduced assumptions and errors, it is considered acceptable if we consider the fact that the interest is to estimate the instability of the slope deposits and not to consider the landslides affecting the bedrock. Furthermore, the analysis has been conducted considering search volumes between 10^5 and 10^7 m^3, in order to neglect smaller and more localised instability phenomena.

4. Results

4.1. Geological-mechanical stratigraphy of the slope

The slope analysed in this work is made up of fairly fine material (light brown silty-sandy clays), with the presence of coarser material, such as angular breccias of different sizes and lithological characteristics. The thickness of this deposit is approximately 20-25 m in the CL10 borehole (Fig. 4). The shallowest part of the slope (<10 m below the ground level) is made up

of very heterogeneous material, from sandy with lenses of gravels, to clast-supported gravels, which have been interpreted as the deposit of the paleo-landslide that covers part of the slope.

Below the light brown silty-sandy clays deposits, there is a level of dark, hardened silty clays, about 5 m thick in the CL10 survey (Fig. 4). In correspondence with the limit between the two units, in the CL10 a sliding surface was identified in the inclinometers, about 32 m below the ground level.

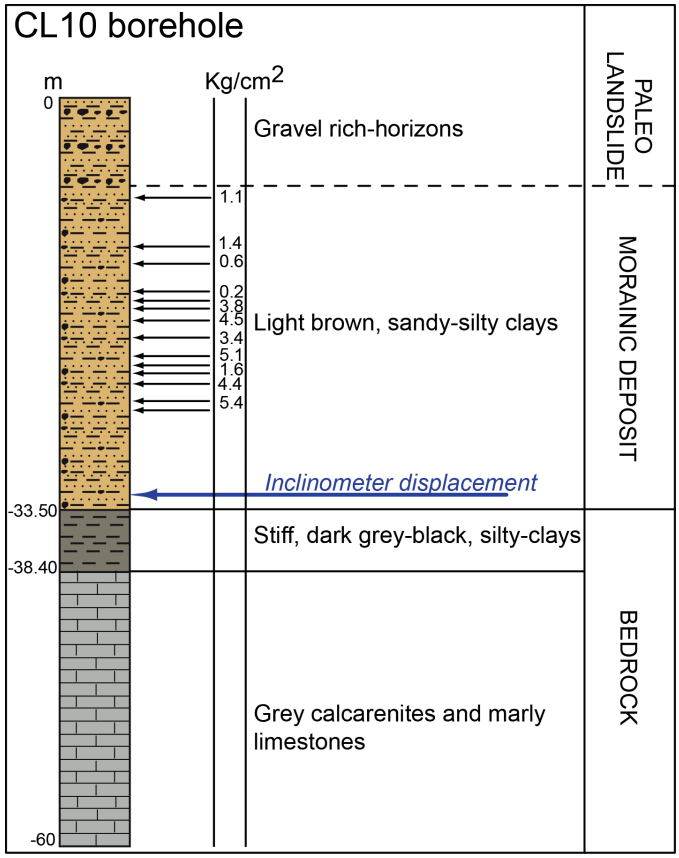

Fig. 4 - Stratigraphy of the CL10 borehole, indicating the lithology and the characteristics detected by scissometric (Torvane) and penetrometric (Pocket Penetrometer) tests. Four lithologies are identified: i) the paleo-landslide, characterised by sands with gravel-rich horizons; ii) a moraine unit, consisting of light-brown sandy-silty clays; iii) stiff, dark grey-black, silty clays; iv) grey calcarenite and marly limestone. The first two levels together form the deposit attributed to the slope (morainic deposits + paleo-landslide), while the two deeper lithologies together form the bedrock.

Below the hardened clayey-silty level, there is a grey calcarenite and marly limestone in CL10.

Based on the characteristics of the material, it has been possible to reconstruct the geotechnical parameters of the material. The slope was divided into 3 units (Table 2):

- a more surficial level, here called “Paleo-landslide”, which corresponds to the sandy deposit with lenses and levels of gravels. The useful parameters for the Mohr-Coulomb failure criterion (φ' and c') have been derived from the bibliography (e.g. Perkins *et al*., 2017);
- a central level, made by light brown silty-sandy clays, called “moraine”, characterised by $\varphi' = 30°$ and $c' = 40$ kPa on average, deriving from the scissometric data;
- a “bedrock”, which includes all the deepest levels of the deposit, to which very high resistance values have been given, assuming that the instability phenomena we are studying are shallower than the bedrock and, therefore, develop in the first two deposits. A GHB (Generalised Hoek-Brown) failure criterion (Hoek *et al*., 2002) was hypothesised for this level.

Table 2 - Geomechanical/geotechnical parameters used for the LEM analysis, following the GHB (Hoek *et al.*, 2002) or the Mohr-Coulomb criterion, *USC* = Uniaxial Compressive Strength of intact rock (Mpa); *GSI* = geological strength index (a-dimensional); m_i = lithological factor (a-dimensional); *D* = disturbance factor (a-dimensional); γ_{unsat} = unsaturated condition unit weight (kN/m^3); γ_{sat} = saturated condition unit weight (kN/m^3).

Geomechanical/geotechnical parameters following the GHB (Hoek *et al.*, 2002) or the Mohr-Coulomb criterion						
Layer	**φ' (°)**	**c' (kPa)**		**γ_{unsat} (kN/m^3)**		**γ_{sat} (kN/m^3)**
Paleo-landslide	20	0		20		21
Moraine	30	40		20		21.5
	UCS (MPa)	*GSI* (-)	m_i (-)	*D* (-)	γ_{unsat} (kN/m^3)	γ_{sat} (kN/m^3)
Bedrock	50	30	12	0	23	25

4.2. Ground displacement

The data deriving from the cost-effective, single frequency GPS network show that the monitored part of the slope has displacements with a NW-SE direction, with predominantly SE-oriented movement (Figs. 5a and 5b). The average horizontal displacement rates are lower (<1.5 m/yr) near the landslide crown, while they reach 1 m/yr towards the central part of the slope, close to the village of Cazzaso (Fig. 5a). The up-down (U-D) movements are negligible in

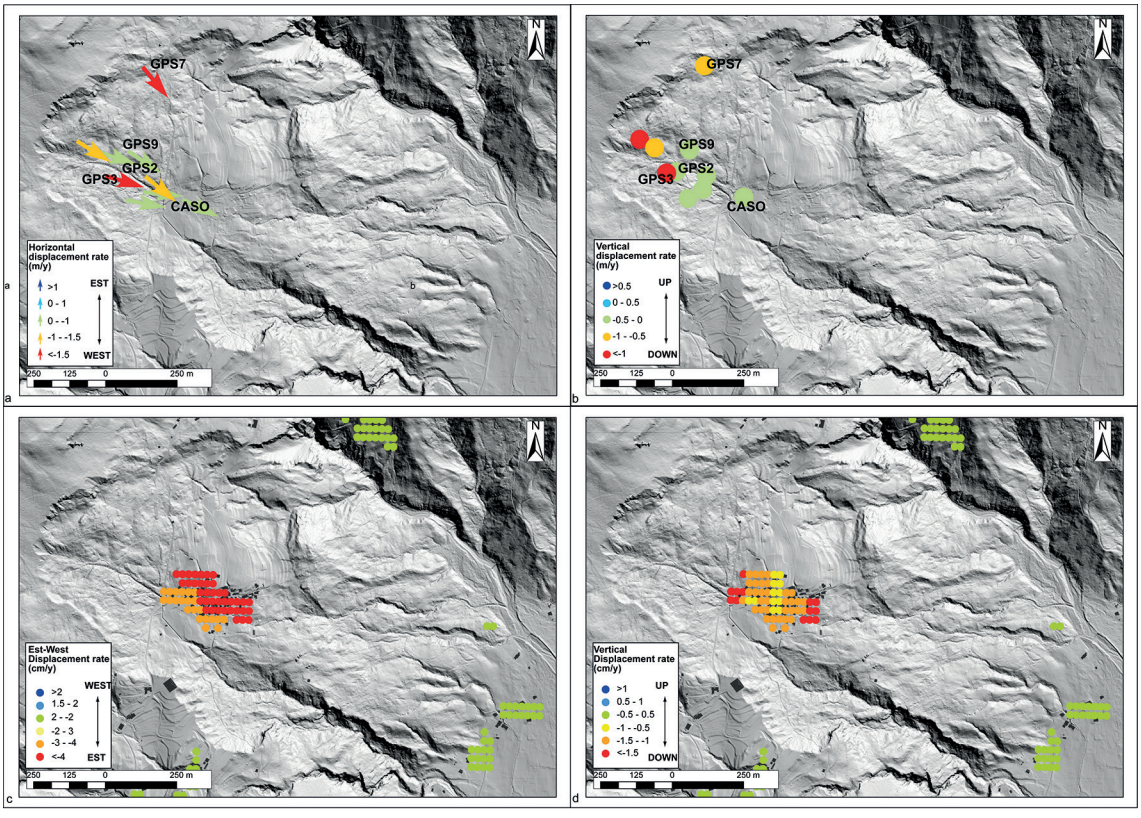

Fig. 5 - Displacement maps from the single frequency GPS network: a) horizontal (E-W) displacement, b) vertical displacement, and from S-1 InSAR data: c) E-W component, d) vertical component.

correspondence with the landslide crown, whereas they are mostly localised in the centre of the slope (Fig. 5b).

InSAR data from S-1 are concentrated on the Cazzaso village and show an eastward and downward displacement trend (Figs. 5c and 5d). The E-W data show an increase in the rate of displacement from west to east, while the U-D data show differential vertical movements within the village, with a more stable central area than the upstream and downstream areas. The rest of the landslide is not monitored by the S-1 InSAR data, given the presence of vegetation on the slope, which does not allow an estimate of the displacements.

4.3. Slope stability

The degree of stability of the slope has been quantified by means of a 2D stability analysis using the LEM on the profiles 1 and 2, in different groundwater and loading conditions (Fig. 6).

For Profile 1, the most unstable sliding surface corresponds to the easternmost part of the slope, delimited upstream by a morphological trench. Here, the OSR map reveals the presence

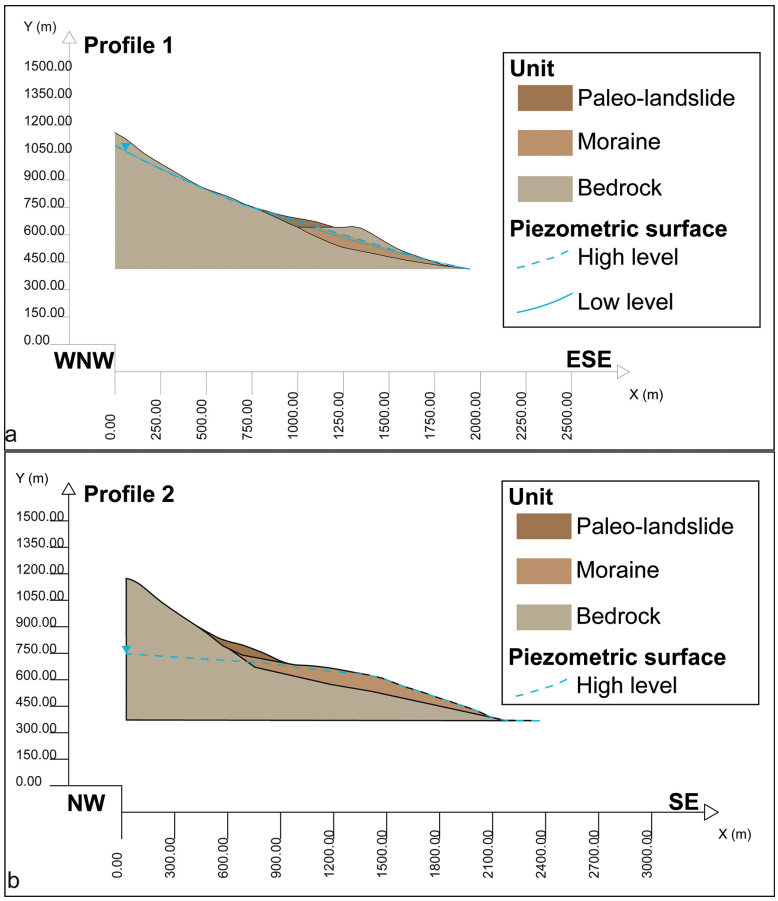

Fig. 6 - Topographic and lithological profiles used for the 2D LEM slope stability analysis. In panel a, two different groundwater settings are introduced, accounting for the low-level and high-level groundwater table, whereas in panel b only a high-level groundwater table is considered. For a better understanding of the location of the profiles, the site of the CASO station has been included in both images.

of a maximum local shear stress greater than the local shear strength. In Fig. 7, it is possible to highlight how the whole slope is in a high stress state, accounting for both the instability of the whole slope and at the same time the possible presence of multiple sliding surfaces. The geometry and location of the areas with high OSR remain the same as the hydrogeological conditions vary, as well as those of seismic load. The only variation is the value of *FS* on the most unstable surface, which changes from values of *FS* = 1.21 to 0.94, revealing a substantial critical stability of the slope unless strong shaking induced by strong earthquakes.

As for Profile 2, the situation is similar to Profile 1. The stability analyses identify a critical surface in the southernmost part of the slope and the presence of high OSR throughout the moraine deposit.

It is, therefore, possible to establish that the entire slope is in critical conditions, therefore compatible with the possible presence of a deep sliding surface, that the most unstable area is the outermost one, and that the internal stress state suggests the possible presence by multiple sliding surfaces.

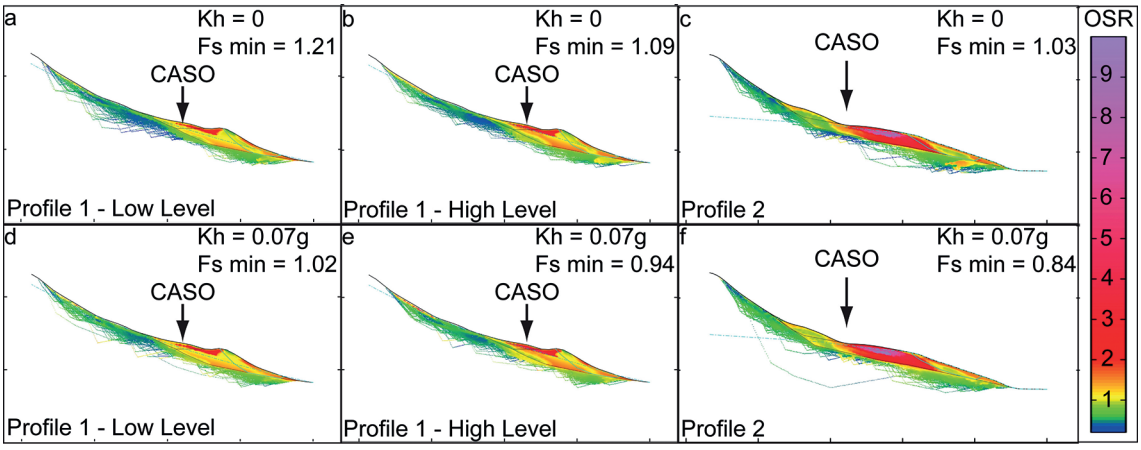

Fig. 7 - Local distribution of the OSR obtained using SSAP software, in different groundwater settings and loading conditions, highlighting the presence of zones of high internal stress, suggesting the possible presence by multiple sliding surfaces.

Considering the results of the 2D analysis, a 3D model of the slope has been created and the 3D LEM analysis has been performed using the Scoops3D software. The analysis has been conducted in the volume range, and the results are expressed in terms of *FS* 3D distribution (Fig. 8). The results in static conditions and full saturation of the deposits reveal the presence of areas with the lowest *FS* (<1.1) in the outermost areas of the slope, in accordance with the results of the 2D analysis. The presence of seismic load increases the area with *FS* <1.1, involving a large part of the slope, including the one where the town of Cazzaso is located.

5. Discussion and conclusive remarks

The results obtained indicate that the studied area is characterised by instability phenomena affecting the entire slope comprised of moraine deposits. The stratigraphic reconstruction

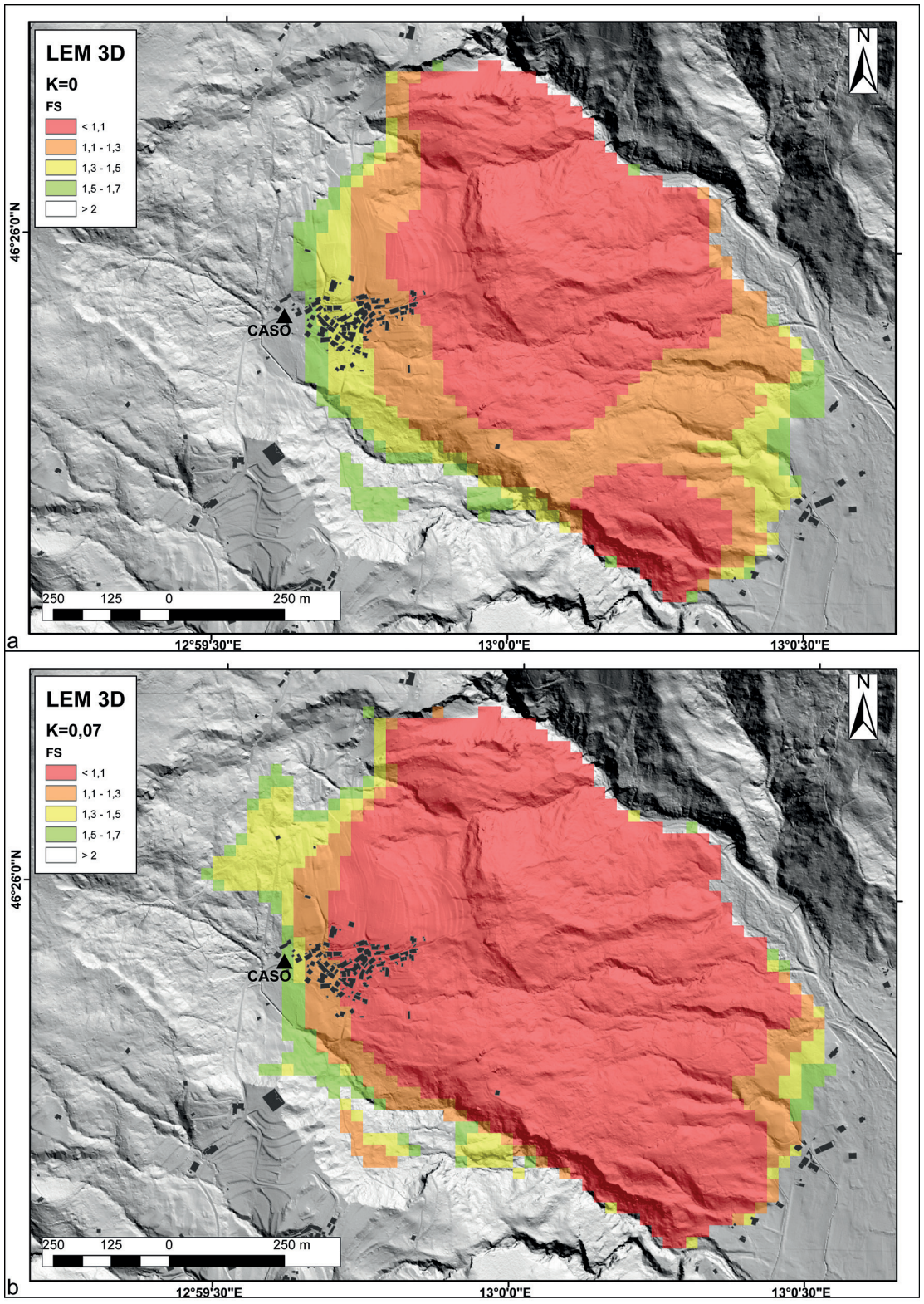

Fig. 8 - Results of the 3D LEM analysis obtained using Scoops3D software, in complete saturated condition: a) no seismic load, b) K_h = 0.07 g. The location of the GNSS reference station CASO has also been reported.

reveals variations in granulometry, distinguishing the material from the paleo-landslide deposits that partially overlay it.

The 2D LEM analysis along different stability profiles highlights areas where the maximum local shear stress exceeds the local shear strength (Fig. 7). This observation, in conjunction with the presence of morphological features such as trenches, counter-slopes, and terracing (see Fig. 2b), suggests that the entire slope is under tension, indicating the occurrence of both deep instability phenomena and multiple shallower surfaces. Examining the local distribution of *FS* (Figs. 7 and 9), it is observed that the potential direction of plasticisation, derived from zones where locally *FS* values fall below 1, aligns with the slope movements recorded by GPS and InSAR data (Fig. 9). The similarity between the data obtained from 2D analytical models and ground displacement data collected by multi-platform sensors confirms the reliability of the LEM model results (Fig. 9).

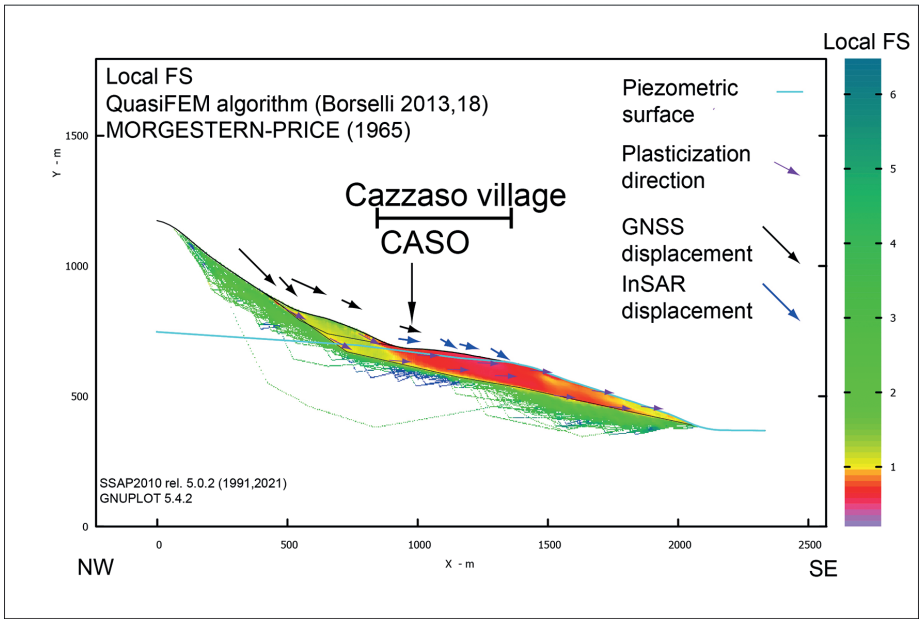

Fig. 9 - Results of the 2D LEM analysis on Profile 2, highlighting the distribution of the local *FS*. The purple **???** arrows represent the likely direction of plasticisation for those areas where *FS* < 1 and the directions are compatible with those derived from displacements measured by GPS sensors and InSAR.

The geological-technical model employed for the 2D modelling is also applied to the 3D models to determine areas with varying susceptibility to failure (Fig. 8). The findings of the 3D analysis align with the 2D results, considering the inherent differences in *FS* calculation and surface identification methods employed by different software. In static conditions (but completely saturated, therefore extreme in terms of distribution of the piezometric surface), it is observed that the village of Cazzaso is only partially located within a highly unstable area (identified here with *FS* values below 1.1, accounting for any uncertainties inherent in the model). The most unstable areas are situated to the east and south of the slope, confirming the results of stability analyses conducted on profiles 1 and 2.

Pseudo-static analyses, with reference coefficients of seismic action *Kh* = 0.07 g and *Kv* = 0.035 g, reveal destabilisation across a significant portion of the slope, with *FS* values below

1 encompassing the entire eastern and southern sectors of the village of Cazzaso. These results are consistent with dynamic analyses conducted using SSAP, wherein the most critical failure surfaces yield *FS* values below 1.

To validate the results of the 3D analysis, a 2D calculation of the *FS* of individual surfaces was carried out (Fig. 10). Surface 1 defines the deposits of the paleo-landslide at the base and intersects the topographical surface in correspondence with the Cazzaso village (Fig. 10a). Surface 2 delimits the entire slope (Fig. 10b), while Surface 3 involves only the moraine deposits (Fig. 10c), with the crown in the village of Cazzaso and the foot at the base of the slope, as it would derive from the results of the 3D models.

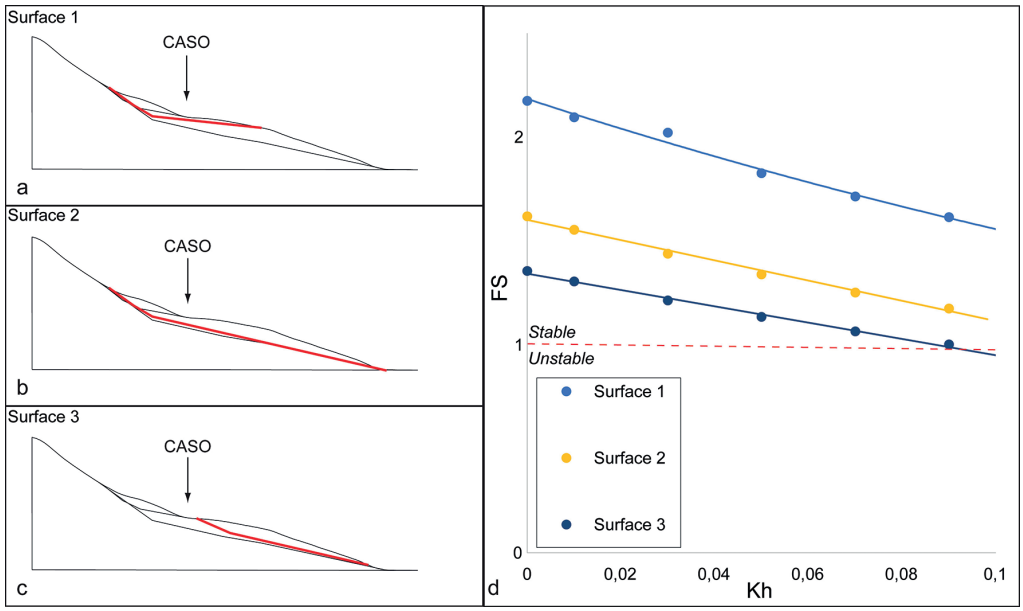

Fig. 10 - Results of the LEM stability analysis conducted on single surfaces in Profile 2, with different seismic load conditions. Surface 3 is the most critical, and at the same time satisfies the constraint imposed by the CL7 and CL10 inclinometers (sliding surface about 30 m below the ground level), the location of which is shown in the figure.

Surfaces 1 and 3 respect the constraint imposed by the CL7 and CL10 inclinometers, i.e. to have a sliding surface located about 30 m below the ground level. On the contrary, Surface 2 represents a deep surface that involves the entire slope. These three surfaces have three different implications: 1) Surface 1 would correspond to the residual movements of the paleo-landslide, which in case of reactivation would impact the town of Cazzaso from upslope; 2) Surface 2 would imply a very large and deep movement, but without large differential movements on the landslide body, with less damage to buildings; 3) the destabilisation of a sector of the slope, with a landslide crown placed in the village of Cazzaso, that would imply strong differential movements even in the case of slow movements of the landslide.

The result of the stability analysis on the individual surfaces revealed that Surface 3 is the one with the lowest *FS* of all three, regardless of the loading conditions (Fig. 10d). This could be the explanation of the identified movements of the CL7 and CL10 inclinometers, and it is in good agreement with the results of the 3D models. Surface 1 is the most stable, even if more detailed checks are necessary, also considering the possible presence of groundwater due to

local hydrogeological conditions, or the presence of soil thicknesses sufficient for the triggering of more superficial phenomena such as soil slip and soil slides, which can turn into debris flows. Data from single-frequency GPS sensors may in part record displacements related to these localised instability conditions. Surface 2, on the other hand, has intermediate values, and it approaches criticality only in conditions of high seismic acceleration.

The approach proposed in this study, which compares analytical models of stability using the LEM in 2D and 3D, along with displacement data obtained from inclinometers, single frequency GPS sensor networks, and InSAR data, enables the mutual validation of model results and interpretation of displacement data. Specifically, the initial 2D stability analysis was supported by the findings of the 3D models. The analytical models were further validated by integrating the displacement data, allowing for the reconstruction of the slope's deformation field. The 2D stability analysis conducted on hypothetical sliding surfaces not only validated the results of the 3D models but also helped interpret the displacement data. It is important to underline, however, that this study does not intend to examine the effects of seismic activity on the Cazzaso landslide. Instead, it focuses on the impact of pore pressure variation in response to water table conditions. The proposed pseudo-static analysis primarily functions to impose an additional constraint on the geotechnical model of the slope. In this scenario, applying a pseudo-horizontal acceleration, similar to that observed during a documented event, enhances the robustness of the geological-technical model employed for slope modelling. A thorough analysis, potentially incorporating dynamic models, would be more appropriate for investigating the site's response to large earthquakes. This approach would encompass not only the possible acceleration but also consider the type of movement.

This methodology confirmed our initial conceptual model, which attributed a significant role to the moraine deposits in the observed instability phenomena. However, the results do not exclude the possibility of deeper sliding surfaces or the activation of shallower surfaces under local conditions that were not extensively analysed in this study. Nevertheless, it can be asserted that the presence of moraine deposits comprising the slope of Cazzaso village, as well as their widespread occurrence in many neighbouring Alpine valleys, represents a primary hazard factor associated with landslides. The findings of this study, both in terms of analysis methodology and results, tailored appropriately to the conditions of each slope characterised by a comparable geological structure, serve as a starting point for mitigating landslide risks in the region, particularly in areas near streams and rivers characterised by morainic deposits in their valleys. It is worth noting that the Alpine valleys, especially those in the south-eastern Alps, have historically experienced frequent instances of river barriers caused by landslides.

Acknowledgments. This paper was partially funded by the IREA CNR/Italian Ministry of Economic Development DGS-UNMIG (now Italian Ministry of Ecology Transition DGISSEG) 2018-2019 agreement. The SSAP software research and development was funded by CONACYT (Mexico): Proyecto Ciencia Basica: CB-2016/286764. Enrico Magrin, Alessio Compagno, Michele Bertoni, Elvio Del Negro, and Paolo Fabris from OGS, are acknowledged for the installation, maintenance, and technical support of the instrumentation, and Gabriele Peressi, from Civil Protection of Friuli Venezia Giulia Region, is acknowledged for the fruitful exchange of information and knowledge on the Cazzaso landslide. The administration of the Municipality of Tolmezzo is acknowledged for the data availability, use, and support during the installation phases. Further information on the solution adopted in this study to manage the cost-effective monitoring network can be found at https://www.yetitmoves.it/. The authors express gratitude to the editors of the journal and the handling editor for overseeing the manuscript. Additionally, appreciation is extended to the two anonymous reviewers for their insightful comments and corrections, which significantly contributed to enhancing the initial version of the manuscript.

REFERENCES

Alejano L.R. and Carranza-Torres C.; 2011: *An empirical approach for estimating shear strength of decomposed granites in Galicia, Spain*. Eng. Geol., 120, 91-102.

Alejano L.R., Gómez-Márquez I. and Martínez-Alegría R.; 2010: *Analysis of a complex toppling-circular slope failure*. Eng. Geol., 114, 93-104.

Alvioli M., Poggi V., Peresan A., Scaini C., Tamaro A. and Guzzetti F.; 2024: *A scenario-based approach for immediate post-earthquake rockfall impact assessment*. Landslides, 21, 1-16.

Anderson H. and Jackson J.; 1987: *Active tectonics of the Adriatic region*. Geophys. J. Int., 91, 937-983.

Barnaba C., Priolo E., Vuan A. and Romanelli M.; 2007: *Site effect of the strong-motion site at Tolmezzo - Ambiesta Dam in northeastern Italy*. Bull. Seismol. Soc. Am., 97, 339-346.

Battaglia M., Zuliani D., Pascutti D., Michelini A., Marson I., Murray M.H. and Burgmann R.; 2003: *Network assesses earthquake potential in Italy's Southern Alps*. EOS, 84, 262-264.

Baum R.L., Coe J.A., Godt J.W., Harp E.L., Reid M.E., Savage W.Z., Schulz W.H., Brien D.L., Chleborad A.F., McKenna J.P. and Michael J.A.; 2005: *Regional landslide-hazard assessment for Seattle, Washington, USA*. Landslides, 2, 266-279, doi: 10.1007/s10346-005-0023-y.

Berardino P., Fornaro G., Lanari R. and Sansosti E.; 2002: *A new algorithm for surface deformation monitoring based on small baseline differential SAR Interferograms*. IEEE Trans. Geosci. Remote Sens., 40, 2375-2383.

Borselli L.; 2022: *SSAP 2010 - Slope stability analysis program, Reference Manual/Manuale di Riferimento, Versione 5.1*. 485 pp., doi: 10.13140/RG.2.2.31522.91841.

Borselli L., Capra L., Sarocchi D. and De la Cruz-Reyna S.; 2011: *Flank collapse scenarios at Volcán de Colima, Mexico: a relative instability analysis*. J. Volcanol. Geotherm. Res., 208, 51-65.

Bragato P.L., Comelli P., Saraò A., Zuliani D., Moratto L., Poggi V., Rossi G., Scaini C., Sugan M., Barnaba C., Bernardi P., Bertoni M., Bressan G., Compagno A., Del Negro A., Di Bartolomeo P., Fabris P., Garbin M., Grossi M., Magrin A., Magrin E., Pesaresi D., Petrovic B., Plasencia Linares M.P., Romanelli M., Snidarcig A., Tunini L., Urban S., Venturini E. and Parolai S.; 2021: *The OGS - Northeastern Italy seismic and deformation network: current status and outlook*. Seismol. Res. Lett., 92, 1704-1716.

Brime C., Perri M.C., Pondrelli M., Spalletta C. and Venturini C.; 2008: *Polyphase metamorphism in the eastern Carnic Alps (N Italy - S Austria): clay minerals and conodont colour alteration index evidence*. Int. J. Earth Sci., 97, 1213-1229.

Carton A., Bondesan A., Fontana A., Meneghel M., Miola A., Mozzi P., Primon S. and Surian N.; 2009: *Geomorphological evolution and sediment transfer in the Piave River system (northeastern Italy) since the Last Glacial Maximum*. Géomorphol.: relief, processus, environnement, 15, 155-174, doi: 10.4000/geomorphologie.7639.

Carturan L., Baldassi G.A., Bondesan A., Calligaro S., Carton A., Cazorzi F., Dalla Fontana G., Francese R., Guarnieri A. and Milan N.; 2013: *Current behaviour and dynamics of the lowermost Italian glacier (Montasio Occidentale, Julian Alps)*. Geografiska Annaler: Series A, Physical Geography, 95, 79-96.

Castellarin A. and Cantelli L.; 2000: *Neo-Alpine evolution of the southern Eastern Alps*. J. Geodyn., 30, 251-274.

Casu F. and Manconi A.; 2016: *Four-dimensional surface evolution of active rifting from spaceborne SAR data*. Geosphere, 12, 1-9, doi: 10.1130/GES01225.1.

Casu F., Elefante S., Imperatore P., Zinno I., Manunta M., De Luca C. and Lanari R.; 2014: *SBAS-DInSAR parallel processing for deformation time-series computation*. IEEE J. Sel. Top. Appl. Earth Obs. Remote Sens., 7, 3285-3296.

CNR-GNDCI (Consiglio Nazionale delle Ricerche, Gruppo Nazionale per la Difesa dalle Catastrofi Idrogeologiche); 1992: *Progetto AVI (Aree Vulnerate Italiane), Catalogo delle informazioni sulle località italiane colpite da frane e da inondazioni*. Scheda di Censimento n. 1300218, < wwwdb.gndci.cnr.it/php2/avi/frane_tutto.php?numero_frana=1300218&lingua=it>.

Colucci R.R., Monegato G. and Žebre M.; 2014: *Glacial and proglacial deposits of the Resia Valley (NE Italy): new insights on the onset and decay of the last Alpine Glacial Maximum in the Julian Alps*. Alp. Mediterr. Quat., 27, 85-104.

Colucci R.R., Boccali C., Žebre M. and Guglielmin M.; 2016: *Rock glaciers, protalus ramparts and pronival ramparts in the south-eastern Alps*. Geomorph., 269, 112-121.

Desio A.; 1926: *L'evoluzione morfologica del bacino della Fella in Friuli*. Atti della Società italiana di Scienze Naturali e del Museo Civico di Storia Naturale di Milano, 55, 205-461.

Di Traglia F., Borselli L., Nolesini T. and Casagli N.; 2023a: *Crater-rim collapse at Stromboli volcano: understanding*

the mechanisms leading from the failure of hot rocks to the development of glowing avalanches. Nat. Hazard, 115, 2051-2068.

Di Traglia F., Calvari S., Borselli L., Cassanego L., Giudicepietro F., Macedonio G., Nolesini T. and Casagli N.; 2023b: *Assessing flank instability of Stromboli Volcano (Italy) by reappraising the 30 December 2002 tsunamigenic landslides*. Landslides, 20, 1363-1380.

Ehlers J. and Gibbard P.L.; 2004: *Quaternary glaciations - Extent and chronology. Part I: Europe (second ed.).* Elsevier, Amsterdam, The Netherlands, 475 pp.

Fan X., Dufresne A., Subramanian S.S., Strom A., Hermanns R., Stefanelli C.T., Hewitt K., Yunus A.P., Dunning S., Capra L., Geertsema M., Miller B., Casagli N., Jansen J.D. and Xu Q.; 2020: *The formation and impact of landslide dams - State of the art.* Earth Sci. Rev., 203, 103116, 85 pp., doi: 10.1016/j.earscirev.2020.103116.

Farias M.M. and Naylor D.J.; 1998: *Safety analysis using finite elements*. Comput. Geotech., 22, 165-181.

Gao Y., Yang W., Guo R. and Jiang L.; 2023: *Remote sensing monitoring and analysis of Jinwuco lateral moraine landslide - glacial lake outburst in southeast Tibet*. Remote Sens., 15, 1475, 18 pp., doi: 10.3390/rs15061475.

Govi M.; 1977: *Photo-interpretation and mapping of the landslides triggered by the Friuli earthquake (1976)*. Bull. Int. Assoc. Eng. Geol., 15, 67-72, doi: 10.1007/BF02592650.

Griffiths D.V. and Lane P.A.; 1999: *Slope stability analysis by finite elements*. Geotech., 49, 387-403.

Hoek E., Carranza-Torres C. and Corkum B.; 2002: *Hoek-Brown failure criterion - 2002 edition*. In: Proc. NARMS-Tac Conference, Toronto, Canada, 1, pp. 267-273.

Hofmann-Wellenhof B., Lichtenegger H. and Collins J.; 2001: *Applications of GPS.* In: Global Positioning System, Springer, Vienna, Austria, pp. 319-343.

Innocenti A., Pazzi V., Borselli L., Nocentini M., Lombardi L., Gigli G. and Fanti R.; 2023: *Reconstruction of the evolution phases of a landslide by using multi-layer back-analysis methods*. Landslides, 20, 189-207.

Jaeger J.C., Cook N.G.W. and Zimmerman R.; 2007: *Fundamentals of Rock Mechanics, 4th ed*. Wiley-Blackwell Publishing, Hoboken, NJ, USA, 488 pp., doi: 10.1017/CBO9780511735349.

Kaplan E.D. and Hegarty C.J. (eds); 1996: *Understanding GPS: principles and applications*. Artech House Inc., Norwood, MA, USA, 723 pp.

Klimeš J., Novotný J., Novotná I., de Urries B.J., Vilímek V., Emmer A., Strozzi T., Kusák M., Rapre A.C., Hartvich F. and Frey H.; 2016: *Landslides in moraines as triggers of glacial lake outburst floods: example from Palcacocha Lake (Cordillera Blanca, Peru)*. Landslides, 13, 1461-1477.

Korup O. and Tweed F.; 2007: *Ice, moraine and landslide dams in mountainous terrain*. Quat. Sci. Rev., 26, 3406-3422, doi: 10.1016/j.quascirev.2007.10.012.

Magrin A. and Rossi G.; 2020: *Deriving a new crustal model of northern Adria: the northern Adria Crust (NAC) model*. Front. Earth Sci., 8, 89, 25 pp., doi: 10.3389/feart.2020.00089.

Manunta M., De Luca C., Zinno I., Casu F., Manzo M., Bonano M., Fusco A., Pepe A., Onorato G., Berardino P., De Martino P. and Lanari R.; 2019: *The parallel SBAS approach for Sentinel-1 interferometric wide swath deformation time - series generation: algorithm description and products quality assessment*. IEEE Trans. Geosci. Remote Sens., 57, 9, 23 pp., doi: 10.1109/TGRS.2019.2904912.

Mayne P.W.; 2001: *Stress-strain-strength-flow parameters from enhanced in-situ tests*. In: Proc. International Conference on In-Situ Measurement of Soil Properties & Case Histories (In-Situ 2001), Bali, Indonesia, pp. 27-48.

Monegato G., Ravazzi C., Donegana M., Pini R., Calderoni G. and Wick L.; 2007: *Evidence of a two-fold glacial advance during the last glacial maximum in the Tagliamento end moraine system (eastern Alps)*. Quat. Res., 68, 284-302, doi: 10.1016/j.yqres.2007.07.002.

Morgenstern N.U. and Price V.E.; 1965; *The analysis of the stability of general slip surfaces*. Geotech., 15, 79-93.

Novotný J. and Klimeš J.; 2014: *Grain size distribution of soils within the Cordillera Blanca, Peru: an indicator of basic mechanical properties for slope stability evaluation*. J. Mountain Sci., 11, 563-577.

Pánek T., Schönfeldt E., Winocur D., Břežný M., Šilhán K., Chalupa V. and Korup O.; 2020: *Moraines and marls: giant landslides of the Lago Pueyrredón valley in Patagonia, Argentina*. Quat. Sci. Rev., 248, 106598, 15 pp., doi: 10.1016/j.quascirev.2020.106598.

Pasquaré Mariotto F. and Venturini C.; 2019: *Birth and evolution of the Paleocarnic Chain in the Southern Alps: a review*. Int. J. Earth Sci., 108, 2469-2492.

Paulin G.L., Mickelson K.A., Contreras T.A., Gallin W., Jacobacci K.E. and Bursik M.; 2022: *Assessing landslide volume using two generic models: application to landslides in Whatcom County, Washington, USA*. Landslides, 19, 901-912.

Perkins J.P., Reid M.E. and Schmidt K.M.; 2017: *Control of landslide volume and hazard by glacial stratigraphic architecture, northwest Washington State, USA*. Geol., 45, 1139-1142.

Pondrelli M., Corradini C., Spalletta C., Simonetto L., Perri M.C., Corriga M.G., Venturini C. and Schönlaub H.P.; 2020: *Geological map and stratigraphic evolution of the central sector of the Carnic Alps (Austria-Italy)*. Ital. J. Geosci., 139, 469-484.

Reid M.E., Christian S.B. and Brien D.L.; 2000: *Gravitational stability of three-dimensional stratovolcano edifices*. J. Geophys. Res., Solid Earth, 105, 6043-6056.

Reid M.E., Christian S.B., Brien D.L. and Henderson S.T.; 2015: *Scoops3D - software to analyze three-dimensional slope stability throughout a digital landscape*. U.S. Geological Survey, Reston, VA, USA, Techniques and Methods, Report 14-A1, 232 pp., doi: 10.3133/tm14A1.

Rossi G., Zuliani D. and Fabris P.; 2016: *Long-term GNSS measurements from the northern Adria microplate reveal fault-induced fluid mobilization.* Tectonophysics, 690, 142–159.

Rossi G., Fabris P. and Zuliani D.; 2018: *Overpressure and fluid diffusion causing non-hydrological transient GNSS displacements*. Pure Appl. Geophys., 175, 1869-1888.

Scaini A., Stritih A., Brouillet C. and Scaini C.; 2021: *Flood risk and river conservation: mapping citizen perception to support sustainable river management*. Front. Earth Sci., 9, 9675131, 14 pp., doi: 10.3389/feart.2021.675131.

Serandrei Barbero R., Rabagliati R. and Zecchetto S.; 1989: *Analisi delle misure alle fronti dei ghiacciai delle Alpi Giulie e correlazioni con i dati climatici*. Geogr. Fis. Din. Quat., 12, 139-149.

Schofield A. and Wroth P.; 1968: *Critical state soil mechanics.* McGraw-Hill, London, U.K., 310 pp.

Shulmeister J., Davies T.R., Evans D.J., Hyatt O.M. and Tovar D.S.; 2009: *Catastrophic landslides, glacier behaviour and moraine formation - A view from an active plate margin*. Quat. Sci. Rev., 28, 1085-1096.

Slejko D., Carulli G.B., Riuscetti M., Cucchi F., Grimaz S., Rebez A. and Zini L.; 2011: *Soil characterization and seismic hazard maps for the Friuli Venezia Giulia region (NE Italy)*. Boll. Geof. Teor. Appl., 52, 59-104.

Springman S.M., Jommi C. and Teysseire P.; 2003: *Instabilities on moraine slopes induced by loss of suction: a case history*. Géotech., 53, 3-10.

Tunini L., Magrin A., Rossi G. and Zuliani D.; 2024: *GNSS time series and velocities about a slow convergent margin processed on HPC clusters: products and robustness evaluation*. Earth Syst. Sci. Data, 16, 1083-1106, doi: 10.5194/essd-16-1083-2024.

Ubertini L.; 1990: *Rischio idrogeologico-Attività del Gruppo Nazionale Difesa Catastrofi Idrogeologiche (GNDCI).* In: Atti XX Incontro Centro Studi di Estimo e di Economia Territoriale, 2 marzo 1990, pp. 237-249.

Venturini C. and Discenza K.; 2020: *Friuli (NE Italy): a reference territory for Quaternary River catches and barrier lakes*. Mem. Descr. Carta Geol. d'It., 107, 225-250.

Zinno I., Elefante S., Mossucca L., De Luca C., Manunta M., Terzo O., Lanari R. and Casu F.; 2015: *A first assessment of the P-SBAS DInSAR algorithm performances within a cloud computing environment*. IEEE J. Sel. Topics Appl. Earth Obs. Remote Sens., 8, 4675-4686.

Zinno I., Casu F., De Luca C., Elefante S., Lanari R. and Manunta M.; 2017: *A cloud computing solution for the efficient implementation of the P-SBAS DInSAR approach*. IEEE J. Sel. Top. Appl. Earth Obs. Remote Sens., 10, 802-817, doi: 10.1109/JSTARS.2016.2598397.

Zuliani D., Fabris P. and Rossi G.; 2018: *FReDNet: evolution of a permanent GNSS receiver system*. In: Cefalo R., Zieliński J. and Barbarella M. (eds), New Advanced GNSS and 3D Spatial Techniques, Lecture Notes in Geoinformation and Cartography, Springer, Cham, Switzerland, pp. 123-137.

Zuliani D., Tunini L., Di Traglia F., Chersich M. and Curone D.; 2022a: *Cost-effective, single-frequency GPS network as a tool for landslide monitoring*. Sens., 22, 3526, 11 pp., doi: 10.3390/s22093526.

Zuliani D., Tunini L., Severin M., Bertoni M., Ponton C. and Parolai S.; 2022b: *LZER0: a cost-effective multi-purpose GNSS platform*. Sens., 22, 8314, 15 pp., doi: 10.3390/s22218314.

Corresponding author: Federico Di Traglia
Osservatorio Vesuviano, Istituto Nazionale di Geofisica e Vulcanologia
Via Diocleziano 328, 80124, Napoli, Italy
Phone: +39 3408106121; e-mail: federico.ditraglia@ingv.it